Collaborative Beamforming for Distributed Wireless Ad Hoc Sensor Networks

Hideki Ochiai*
Division of Physics, Electrical and Computer Engineering, Yokohama National University
79-5 Tokiwadai, Hodogaya-ku, Yokohama, Japan 240-8501
Tel: +81-45-339-4116 Fax: +81-45-338-1157 Email: hideki@ynu.ac.jp

Patrick Mitran
Division of Engineering and Applied Sciences, Harvard University
33 Oxford Street, Cambridge, MA 02138
Tel: +1-617-285-9461 Fax: +1-617-496-6404 Email: mitran@deas.harvard.edu

H. Vincent Poor
Department of Electrical Engineering, Princeton University
Princeton, NJ 08544
Tel: +1-609-258-1816 Fax: +1-609-258-1468 Email: poor@princeton.edu

Vahid Tarokh
Division of Engineering and Applied Sciences, Harvard University
33 Oxford Street, Cambridge, MA 02138
Tel: +1-617-384-5026 Fax: +1-617-496-6404 Email: vahid@deas.harvard.edu

Abstract

The performance of collaborative beamforming is analyzed using the theory of random arrays. The statistical average and distribution of the beampattern of randomly generated phased arrays is derived in the framework of wireless ad hoc sensor networks. Each sensor node is assumed to have a single isotropic antenna and nodes in the cluster collaboratively transmit the signal such that the signal in the target direction is coherently added in the far-field region. It is shown that with N sensor nodes uniformly distributed over a disk, the directivity can approach N, provided that the nodes are located sparsely enough. The distribution of the maximum sidelobe peak is also studied. With the application to ad hoc networks in mind, two scenarios, closed-loop and open-loop, are considered. Associated with these scenarios, the effects of phase jitter and location estimation errors on the average beampattern are also analyzed.

EDICS – 1-STAP

*Corresponding author

I. Introduction

Recent advances in the construction of low cost, low power, and mass produced micro sensors and micro-electro-mechanical (MEM) systems have ushered in a new era in system design using distributed sensor networks [1, 2]. The advent of sensor network technology provides a variety of applications that have been considered unrealistic in the past. One such application is in the area of space communications: with ad hoc sensor networks, a number of sensor nodes randomly placed on a planet can collaboratively collect information and then, also collaboratively, send the information back to Earth. In this scenario, the sensors must have an ability to transmit information over very long distances with high energy efficiency. In this kind of point-to-point communication, directional antennas are a preferred means to avoid interference.

In general, this can be achieved by adaptive beamforming. Given a number of well-designed antenna elements at the transmitting/receiving sensor nodes, each node could in principle autonomously transmit/receive the information to/from any desired direction. The advantages and applications of beamforming with antenna arrays are well known; in wireless communications, this enables Space-Division Multiplex Access (SDMA), a technology which has the potential to significantly increase the capacity of the multiple access channel.

One of the most important constraints on wireless sensors is energy efficiency. Since the sensor nodes are often distributed in places where manual maintenance is costly, such as remote locations, on top of buildings and so on, it should be possible to operate these for several months without battery replacement. Considering the fact that each antenna element requires analog circuitry (and thus leads to costly hardware), in practice each distributed sensor is likely equipped with only a single antenna and this precludes the use of autonomous beamforming in scenarios of very energy efficient communication. Nevertheless, if the sensors in the cluster share the information *a priori* and synchronously transmit the data collaboratively as sketched in Fig. 1, it may be possible to beamform when transmitting (and also receiving) the data in a distributed manner. The resultant overhead due to intra-cluster information sharing may be relatively small as this can be done by low-cost short distance broadcasting-type communication among nodes. Thus, with distributed collaborative beamforming, the nodes can send the collected information to the far-end receiver over long distances with high efficiency. Also, only the sensor cluster in the specified target direction receives the data with high signal power and no significant interference occurs for clusters in other directions. Overall there is thus a potential to increase the capacity of the multiple access channel significantly despite the additional overhead for information sharing.

The obvious question is whether one can form a nice beampattern with a narrow mainbeam, or achieve a reasonable directional gain (directivity). The sensor nodes in ad hoc networks are located randomly by nature, and the resultant beampattern depends on the particular realization of the sensor node

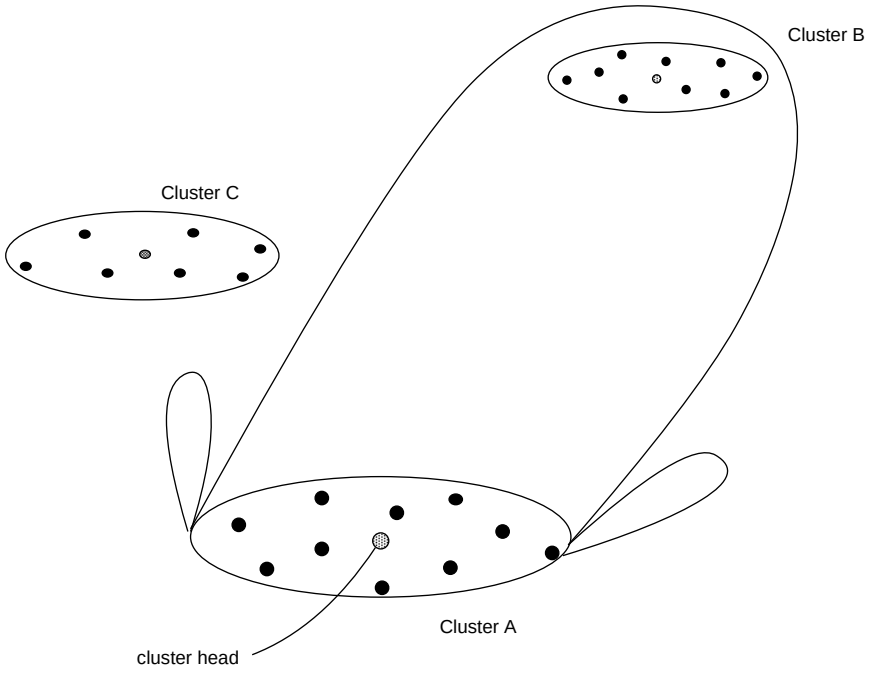

Fig. 1. Collaborative beamforming concept in ad hoc sensor networks.

locations. Therefore, it may be quite natural to treat the beampattern with probabilistic arguments. In this paper, assuming idealized channel model conditions and antenna properties, we analyze the achievable performance of collaborative beamforming based on distributed sensor nodes in a probabilistic sense. Specifically, the statistical properties of the achievable beampattern of the random sensor arrays are studied based on the following assumptions. The sensors form an ad hoc network and the geometry of the cluster is given by a two-dimensional circle of a given radius over which all sensor nodes are distributed uniformly as illustrated in Fig. 1. Since the corresponding far-field beampattern depends on the particular realization of the random array of nodes, the probability distribution of the far-field beampattern is of particular interest.

In the antenna design literature, probabilistic analysis of random arrays is not new. In the framework of linear array design with a large number of sensors, Lo [3] has developed a comprehensive theory of random arrays in the late 1960's, and it has been shown that randomly generated arrays with large numbers of nodes can in fact form a good beampattern with high probability[1]. It has been shown that with N collaborative nodes, the directivity approaches N asymptotically. Although our scenario is quite

[1]The theory of random arrays has been discussed and developed almost exclusively in the antenna design community, e.g., in [3–6]. However, considering that the underlying theory is based on probabilistic approaches, we believe that the ideas behind this work also fall upon the wide interest of the signal processing community.

different in that our main goal is not to design array geometry but to *exploit* the randomness of the distributed sensor network, it turns out that the results we shall develop in this paper can be seen as an extension of the theory of linear random arrays by Lo [3]. Thus, the same conclusion will be reached; with N sensor nodes, one can achieve a directivity of order N asymptotically.

The major difference between classical beamforming by antenna arrays and distributed beamforming is that whereas the geometry of the former is usually known *a priori*, the exact location of the sensor nodes in ad hoc network is not, and it should be acquired dynamically. Even if their relative location is estimated by some adaptive algorithm (e.g., [1] for receiver beamforming), considering the low SNR operation of the sensor nodes, it is highly likely that the acquired geometric information has some inaccuracy. Also, since all nodes are operated with physically different local oscillators, each node may suffer from statistically independent phase offsets. In order to model and investigate the effect of these impairments, we consider the following two scenarios: *closed-loop* and *open-loop*. The closed-loop scenario may be described as follows. Each node independently synchronizes itself to the beacon sent from the destination node (such as a base station) and adjusts its initial phase to it. Thus, the beam will be formed in the direction of arrival of the beacon. This kind of system is often referred to as a *self-phasing* array in the literature, and may be effective for systems operating in time-division duplex (TDD) mode. The residual phase jitter due to synchronization and phase offset estimation among sensor nodes is then often the dominant impairment. On the other hand, in the open-loop scenario we assume that all nodes within the cluster acquire their relative locations from the beacon of a nearby reference point or cluster head. The beam will then be steered toward an arbitrary direction. Thus, the destination need not transmit a beacon, but each node requires precise knowledge of its relative position from a predetermined reference point within the cluster. This case may occur in ad hoc sensor networks where sensor nodes do not have sufficient knowledge of the destination direction *a priori*. In this scenario, the location estimation ambiguity among sensors may also affect the beampattern.

Throughout the paper, the nodes and channel are assumed to be static over the communication period, and for simplicity the information rate is sufficiently low that inter-symbol interference (ISI), due to residual timing offset, is negligible.

It will be also assumed that all nodes share the same transmitting information *a priori*, as the main focus of the paper is on the beampattern, rather than the front-end communication performance.

The paper is organized as follows. Section II describes the assumptions, model, and main parameters that describe beam characteristics. In Section III, the average properties of the beampattern are derived. In Section IV, the statistical distribution of the beampattern in a specific direction is derived. The accuracy of the Gaussian approximation of the array factor, which is a common assumption in the random array literature, is also examined in detail. The distribution of the maximum of the sidelobe region is discussed

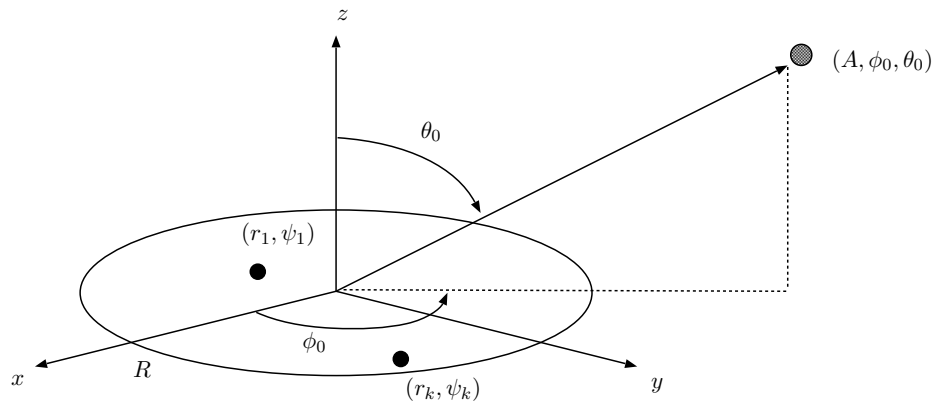

Fig. 2. Definitions of notation.

in Section V, and the effect of phase jitter or location estimation errors on the resultant beampattern is analyzed in Section VI. Finally, Section VII concludes the paper.

II. System Model and Beampattern

The geometrical configuration of the distributed nodes and destination (or target) is illustrated in Fig. 2 where, without loss of generality, all the collaborative sensor nodes are assumed to be located on the x-y plane. The kth node location is thus denoted in polar coordinates by (r_k, ψ_k). The location of the destination is given in spherical coordinates by (A, ϕ_0, θ_0). Following the standard notation in antenna theory [7], the angle $\theta \in [0, \pi]$ denotes the elevation direction, whereas the angle $\phi \in [-\pi, \pi]$ represents the azimuth direction. In order to simplify the analysis, the following assumptions are made:

1) The location of each node is chosen randomly, following a uniform distribution within a disk of radius R.
2) Each node is equipped with a single ideal isotropic antenna.
3) All sensor nodes transmit identical energy, and the path losses of all nodes are also identical. Thus the underlying model falls within the framework of phased arrays.
4) There is no reflection or scattering of the signal. Thus, there is no multipath fading or shadowing.
5) The nodes are sufficiently separated that any mutual coupling effects [7] among the antennas of sensor nodes are negligible.

Furthermore, we also assume that all the nodes are perfectly synchronized so that no frequency offset or phase jitter occurs. The effects of phase ambiguities on the beampattern will be discussed in Section VI.

Let $d_k(\phi, \theta)$ denote the Euclidean distance between the kth node and the reference location (A, ϕ, θ), which is given by

$$d_k(\phi, \theta) = \sqrt{A^2 + r_k^2 - 2 r_k A \sin\theta \cos(\phi - \psi_k)} \ . \tag{1}$$

If the initial phase of the node $k \in \{1, 2, \ldots, N\}$ is set to

$$\Psi_k = -\frac{2\pi}{\lambda} d_k(\phi_0, \theta_0), \tag{2}$$

the corresponding array factor, given the realization of node locations $\boldsymbol{r} = [r_1, r_2, \ldots, r_N] \in [0, R]^N$ and $\boldsymbol{\psi} = [\psi_1, \psi_2, \ldots, \psi_N] \in [-\pi, \pi]^N$, is given by

$$F(\phi, \theta | \boldsymbol{r}, \boldsymbol{\psi}) = \frac{1}{N} \sum_{k=1}^{N} e^{j\Psi_k} e^{j\frac{2\pi}{\lambda} d_k(\phi,\theta)} = \frac{1}{N} \sum_{k=1}^{N} e^{j\frac{2\pi}{\lambda}[d_k(\phi,\theta) - d_k(\phi_0,\theta_0)]} \tag{3}$$

where N is the number of sensor nodes and λ is the wavelength of the radio frequency (RF) carrier.

In this paper, we are interested in the radiation pattern in the far-field region, and we assume that the far-field condition $A \gg r_k$ holds. The far-field distance $d_k(\phi, \theta)$ in (1) can then be approximated as

$$d_k(\phi, \theta) \approx A - r_k \sin\theta \cos(\phi - \psi_k). \tag{4}$$

The far-field beam pattern is thus approximated by

$$F\left(\phi, \theta | \boldsymbol{r}, \boldsymbol{\psi}\right) \approx \frac{1}{N} \sum_{k=1}^{N} e^{j\frac{2\pi}{\lambda} r_k [\sin\theta_0 \cos(\phi_0 - \psi_k) - \sin\theta \cos(\phi - \psi_k)]} \triangleq \tilde{F}(\phi, \theta | \boldsymbol{r}, \boldsymbol{\psi}). \tag{5}$$

Alternatively, if, instead of applying Ψ_k as in (2), we choose

$$\Psi_k^{\dagger} = \frac{2\pi}{\lambda} r_k \sin\theta_0 \cos(\phi_0 - \psi_k), \tag{6}$$

then we obtain the array factor as

$$\begin{aligned} F^{\dagger}(\phi, \theta | \boldsymbol{r}, \boldsymbol{\psi}) &= \frac{1}{N} \sum_{k=1}^{N} e^{j\Psi_k^{\dagger}} e^{j\frac{2\pi}{\lambda} d_k(\phi,\theta)} \\ &\approx \frac{1}{N} \sum_{k=1}^{N} e^{j\frac{2\pi}{\lambda}[A - r_k \sin\theta \cos(\phi - \psi_k) + r_k \sin\theta_0 \cos(\phi_0 - \psi_k)]} \\ &= e^{j\frac{2\pi}{\lambda} A} \frac{1}{N} \sum_{k=1}^{N} e^{j\frac{2\pi}{\lambda} r_k [\sin\theta_0 \cos(\phi_0 - \psi_k) - \sin\theta \cos(\phi - \psi_k)]} \triangleq \tilde{F}^{\dagger}(\phi, \theta | \boldsymbol{r}, \boldsymbol{\psi}). \end{aligned} \tag{7}$$

The only difference between $\tilde{F}(\phi, \theta | \boldsymbol{r}, \boldsymbol{\psi})$ in (5) and $\tilde{F}^{\dagger}(\phi, \theta | \boldsymbol{r}, \boldsymbol{\psi})$ in (7) is the existence of the initial phase offset by $\frac{2\pi}{\lambda} A$. The far-field beampattern is thus identical for both systems, and the received signal exhibits no difference as long as the base station compensates for this phase rotation.

Therefore, there are two ways of forming a beam. One way is to use (2), but this approach requires accurate knowledge of the distance, relative to the wavelength λ, between each node and destination. Thus, this applies to the closed-loop case such as self-phasing arrays. Alternatively, the use of (6) requires knowledge of the node positions relative to some common reference (such as the origin in this example), and thus corresponds to the open-loop case. Knowledge of the elevation direction θ_0 is also required, but this may be assumed to be known *a priori* in many applications. In both cases, the synchronization

among sensors is critical, which may be achieved by the use of reference signals such as those of the Global Positioning System (GPS).

Of particular interest in practice is the case where $\theta = \frac{\pi}{2}$, i.e., the azimuth directivity of the beam, and thus for simplicity we will assume that $\theta = \theta_0 = \frac{\pi}{2}$ for the rest of the paper. Therefore, for simplicity we denote $\tilde{F}(\phi, \theta = \pi/2|\boldsymbol{r}, \boldsymbol{\psi})$ in (5) by $\tilde{F}(\phi|\boldsymbol{r}, \boldsymbol{\psi})$, and $\tilde{F}^{\dagger}(\phi, \theta = \pi/2|\boldsymbol{r}, \boldsymbol{\psi})$ in (7) by $\tilde{F}^{\dagger}(\phi|\boldsymbol{r}, \boldsymbol{\psi})$.

By assumption, the node locations (r_k, ψ_k) follow the uniform distribution over the disk of radius R. Thus, the probability density functions (pdfs) of r_k and ψ_k are given by

$$f_{r_k}(r) = \frac{2r}{R^2}, \quad 0 < r < R, \qquad \text{and} \qquad f_{\psi_k}(\psi) = \frac{1}{2\pi}, \quad -\pi \leq \psi < \pi.$$

From (5), we have (with $\theta = \theta_0 = \pi/2$)

$$\tilde{F}(\phi|\boldsymbol{r}, \boldsymbol{\psi}) = \frac{1}{N} \sum_{k=1}^{N} e^{j\frac{4\pi}{\lambda} r_k \sin\left(\frac{\phi_0 - \phi}{2}\right) \sin\left(\psi_k - \frac{\phi_0 + \phi}{2}\right)} = \frac{1}{N} \sum_{k=1}^{N} e^{j4\pi \frac{R}{\lambda} \sin\left(\frac{\phi_0 - \phi}{2}\right) \tilde{r}_k \sin \tilde{\psi}_k}, \tag{8}$$

where $\tilde{r}_k \triangleq r_k/R$ and $\tilde{\psi}_k \triangleq \psi_k - \frac{\phi_0 + \phi}{2}$. The compound random variable

$$z_k \triangleq \tilde{r}_k \sin \tilde{\psi}_k, \tag{9}$$

has the following pdf:

$$f_{z_k}(z) = \frac{2}{\pi} \sqrt{1 - z^2}, \quad -1 \leq z \leq 1. \tag{10}$$

Note that since the above model is symmetric with respect to the azimuth direction ϕ, the particular choice of ϕ_0 does not change the results in the following. Therefore, without loss of generality, we assume that $\phi_0 = 0$, and the parameter ϕ simply corresponds to the difference angle between the target direction and the reference. Also, note that $|\phi| \leq \pi$.

The array factor of (8) can then be rewritten as

$$\tilde{F}(\phi|\boldsymbol{z}) = \frac{1}{N} \sum_{k=1}^{N} e^{-j4\pi \tilde{R} \sin\left(\frac{\phi}{2}\right) z_k}, \tag{11}$$

where $\tilde{R} \triangleq \frac{R}{\lambda}$ is the radius of the disk normalized by the wavelength.

Finally, the far-field beampattern can be defined as

$$\begin{aligned} P(\phi|\boldsymbol{z}) &\triangleq \left|\tilde{F}(\phi|\boldsymbol{z})\right|^2 = \tilde{F}(\phi|\boldsymbol{z}) \tilde{F}^*(\phi|\boldsymbol{z}) \\ &= \frac{1}{N^2} \sum_{k=1}^{N} \sum_{l=1}^{N} e^{-j4\pi \tilde{R} \sin\left(\frac{\phi}{2}\right)(z_k - z_l)} \\ &= \frac{1}{N} + \frac{1}{N^2} \sum_{k=1}^{N} e^{-j\alpha(\phi) z_k} \sum_{\substack{l=1 \\ l \neq k}}^{N} e^{j\alpha(\phi) z_l} \end{aligned} \tag{12}$$

where

$$\alpha(\phi) \triangleq 4\pi \tilde{R} \sin \frac{\phi}{2}. \tag{13}$$

III. Average Properties of Beampattern of Uniformly Distributed Sensor Array with Perfect Phase Information

A. Average Far-Field Beampattern

We start by investigating the average beampattern of the random array resulting from the distributed sensor network model in the previous section. Here, the average is taken over all realizations of $\boldsymbol{z}$, and from (12) the average beampattern is expressed as

$$P_{\text{av}}(\phi) \triangleq E_{\boldsymbol{z}}\left[P(\phi|\boldsymbol{z})\right], \tag{14}$$

where $E_{\boldsymbol{x}}[\cdot]$ denotes expectation with respect to the random variables $\boldsymbol{x}$. From (12) and (10), it can be readily shown that

$$P_{\text{av}}(\phi) = \frac{1}{N} + \left(1 - \frac{1}{N}\right)\left|2 \cdot \frac{J_1\left(\alpha(\phi)\right)}{\alpha(\phi)}\right|^2, \tag{15}$$

where $J_n(x)$ is the nth order Bessel function of the first kind. Although the function $J_1(x)/x$ is oscillatory, the local maxima of oscillation tend to decrease with increasing x. In (15), the first term represents the average power level of the sidelobe which does not depend on the node location, whereas the second term is the contribution of the mainlobe factor. Since, conditioned on ϕ, the array factor of the form (11) is an average of bounded independent and identically distributed (i.i.d.) complex random variables, as $N \to \infty$, by the strong law of large numbers it approaches the ensemble average (15) with probability one.

The average beampattern of (15) is plotted in Fig. 3 for several values of $\tilde{R}$ with $N = 16$ and 256. As can be observed, the sidelobe approaches $1/N$ as the beam angle moves away from the target direction.

To gain further insight, consider the asymptotic expansion of the Bessel function $J_1(x)$ for $x \gg 1$ as

$$J_1(x) \sim \sqrt{\frac{2}{\pi x}}\cos\left(x - \frac{3}{4}\pi\right). \tag{16}$$

We then have

$$\left|2 \cdot \frac{J_1(x)}{x}\right|^2 \sim \frac{8}{\pi x^3}\cos^2\left(x - \frac{3}{4}\pi\right), \tag{17}$$

and (15) becomes, for $\alpha(\phi) = 4\pi\tilde{R}\sin\left(\frac{\phi}{2}\right) \gg 1$,

$$P_{\text{av}}(\phi) \sim \frac{1}{N} + \left(1 - \frac{1}{N}\right)\frac{8}{\pi\alpha(\phi)^3}\cos^2\left(\alpha(\phi) - \frac{3}{4}\pi\right). \tag{18}$$

The nth peak of the average sidelobe will appear around $\alpha(\phi_n) \approx \left(n - \frac{1}{4}\right)\pi$, $n = 1, 2, \ldots$, and its corresponding value becomes

$$P_{\text{av}}(\phi_n^{\text{peak}}) \sim \frac{1}{N} + \left(1 - \frac{1}{N}\right)\frac{1}{\pi}\left[\frac{2}{\pi\left(n - \frac{1}{4}\right)}\right]^3, \tag{19}$$

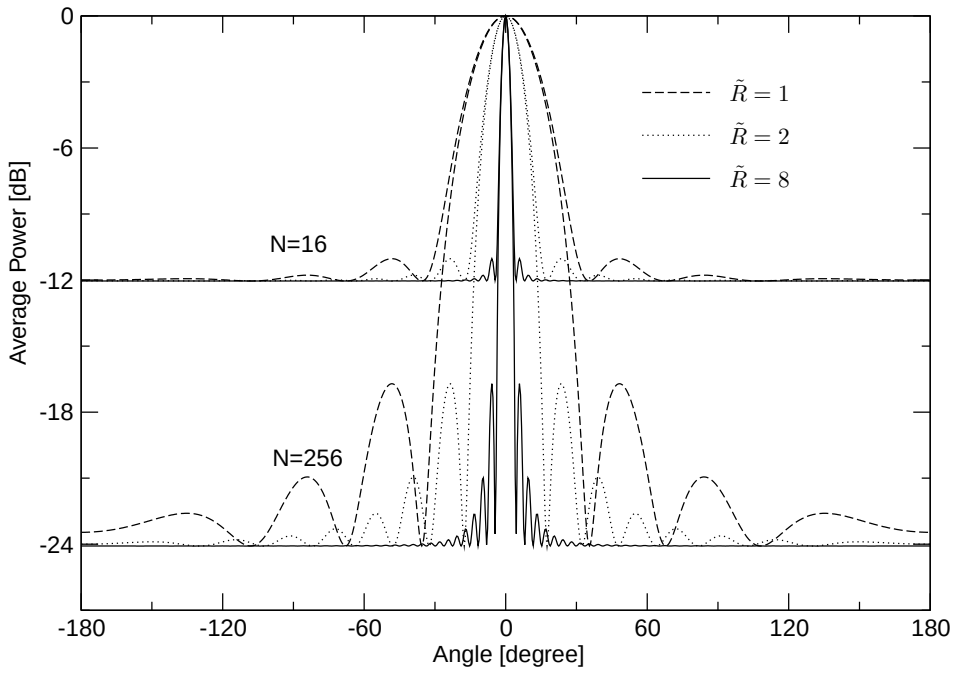

Fig. 3. Average beampattern with different $\tilde{R}$ and $N = 16, 256$.

which does not depend on $\tilde{R}$. On the other hand, the nth peak and nth zero positions (in the sense of the second term in (15)) can be expressed asymptotically as

$$\phi_n^{\text{peak}} \sim 2\arcsin\left(\frac{n-\frac{1}{4}}{4\tilde{R}}\right) \tag{20}$$

$$\phi_n^{\text{zero}} \sim 2\arcsin\left(\frac{n+\frac{1}{4}}{4\tilde{R}}\right). \tag{21}$$

Since the peak sidelobe value does not depend on $\tilde{R}$ and is less sensitive to the value of N, it is apparent that the only way one can avoid high peaks in the sidelobe region is to increase $\tilde{R}$ such that most of the major peaks are relatively concentrated around the mainlobe. This phenomenon will be further examined in the following subsection.

B. 3 dB Beamwidth of the Average Beampattern

One of the important figures of merit in directional antenna design is the 3 dB beamwidth. In the deterministic antenna, the 3 dB beamwidth is the threshold angle at which the power of the beampattern drops 3 dB below that in the target direction ϕ_0. In our scenario, the 3 dB beamwidth itself is a random variable and it is not easy to characterize analytically. Thus, as an alternative measure, we may define the 3dB beamwidth of the *average* beampattern denoted by $\phi_{\text{av}}^{\text{3dB}}$ as the angle ϕ that satisfies

$$P_{\text{av}}(\phi_{\text{av}}^{\text{3dB}}) = \frac{1}{2}. \tag{22}$$

In the limit as $N \to \infty$, one may obtain

$$\phi_{\text{av}}^{\text{3dB}} = 2 \arcsin\left(\frac{0.1286}{\tilde{R}}\right), \tag{23}$$

by numerically solving (15). For $\tilde{R} \gg 1$, (23) can be approximated as $\phi_{\text{av}}^{\text{3dB}} \approx 0.26/\tilde{R}$. Therefore, the beamwidth is asymptotically independent of N and is mainly determined by the inverse of the circle radius of the cluster. Consequently, sparsely distributed sensors tend to form a narrow beam on average.

This sharp mainbeam property may be desirable, but if the far-field destination node has mobility, it should be designed carefully; the calibration should take place before the mobile node moves out of the mainbeam, but the mainbeam width is inversely proportional to the normalized radius $\tilde{R}$ as observed in Fig. 3. Therefore, calibration should be performed more frequently if the destination node moves rapidly or when $\tilde{R}$ is increased.

C. 3 dB Sidelobe Region

Similar to the 3 dB beamwidth concept, it may be also convenient for our subsequent analysis to define the region within which the average of the sidelobe beampattern falls below some threshold level. As we have seen, for large $\tilde{R}$, the sidelobe of the average beampattern is given by $1/N$ asymptotically. Therefore, we shall define the *3 dB sidelobe region* as the region in which neither neighboring sidelobe peak in the average beampattern exceeds 3 dB above $1/N$. Let n_0 denote the minimum index of the peak position such that the corresponding peak value satisfies this 3 dB condition. Specifically, from (19), n_0 is the minimum integer n that satisfies

$$\frac{P_{\text{av}}(\phi_n^{\text{peak}})}{1/N} \sim 1 + (N-1)\,\frac{1}{\pi}\left[\frac{2}{\pi\left(n-\frac{1}{4}\right)}\right]^3 \leq 2, \tag{24}$$

and it can be bounded by

$$n_0 \geq \frac{1}{4} + \frac{2}{\pi}\left(\frac{N-1}{\pi}\right)^{\frac{1}{3}}. \tag{25}$$

Let $\phi_{n_0}^{\text{zero}} > 0$ denote the angle corresponding to the zero point next to the n_0th peak sidelobe which can be obtained by (21) with $n = n_0$. Consequently, in this paper, the 3 dB sidelobe region is defined as

$$\mathcal{S}_{\text{3dB}} \triangleq \left\{\phi \;\middle|\; \pi \geq |\phi| \geq \phi_{n_0}^{\text{zero}}\right\}. \tag{26}$$

Fig. 4 illustrates the definitions of the 3 dB sidelobe region together with that of the 3 dB beamwidth.

The idea behind the introduction of 3 dB sidelobes is that in this region one may assume that the mean value of the random array factor of (8) sampled at $\phi \in \mathcal{S}_{\text{3dB}}$ becomes a random variable with approximately zero mean, as will be shown in Section IV-C. Thus we may reasonably assume that the array factor has zero mean in this region, and this assumption significantly simplifies the analysis of the statistical distribution in the following sections.

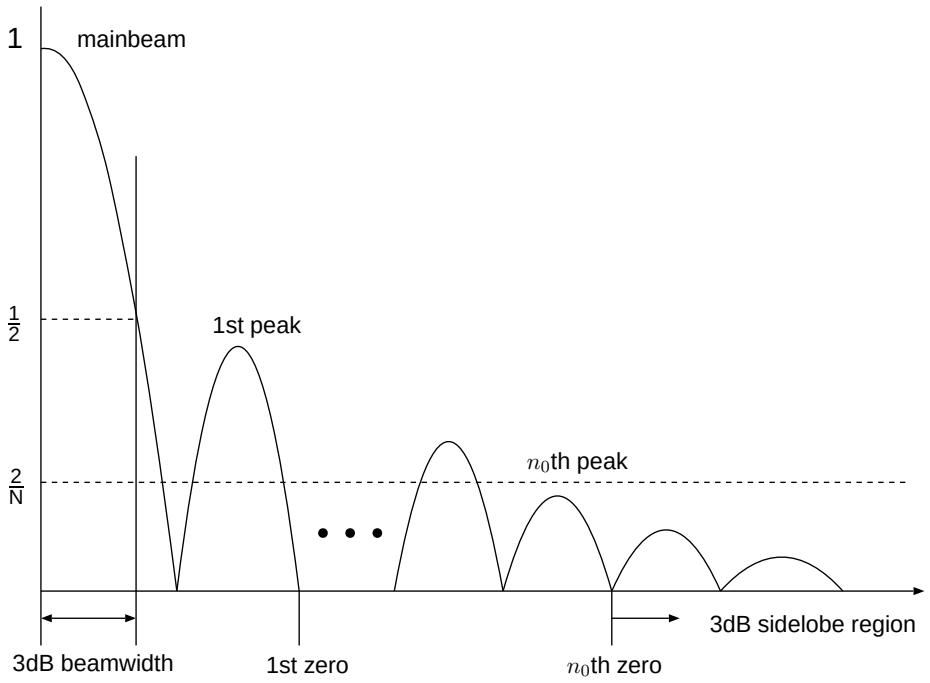

Fig. 4. Definitions of 3 dB beamwidth and 3 dB sidelobe region.

Fig. 5 shows the threshold angle above which the 3 dB sidelobe region begins. The asymptotic 3 dB beamwidth (23) is also shown for reference. As can be observed, whereas the 3 dB beamwidth is less sensitive to the number of nodes N, the 3 dB sidelobe region will be considerably reduced as N increases. This means that as N increases the dominant non-negligible sidelobe peak may occur with high probability unless $\tilde{R}$ is also increased. This trade-off will be clarified by the study of directivity in the following subsection.

D. Average Directivity

The directivity or directional gain is the parameter that characterizes how much radiated energy is concentrated in the desired direction, relative to a single isotropic antenna. Specifically, it may be defined as

$$D \triangleq \frac{\int_{-\pi}^{\pi} P(0)d\phi}{\int_{-\pi}^{\pi} P(\phi)d\phi} = \frac{2\pi}{\int_{-\pi}^{\pi} P(\phi)d\phi}, \tag{27}$$

where $P(\phi)$ is the radiated power density in the direction of ϕ. In the scenario of this paper, since $P(\phi)$ depends on the particular realization of $\boldsymbol{z}$, the corresponding gain may be expressed, by substituting

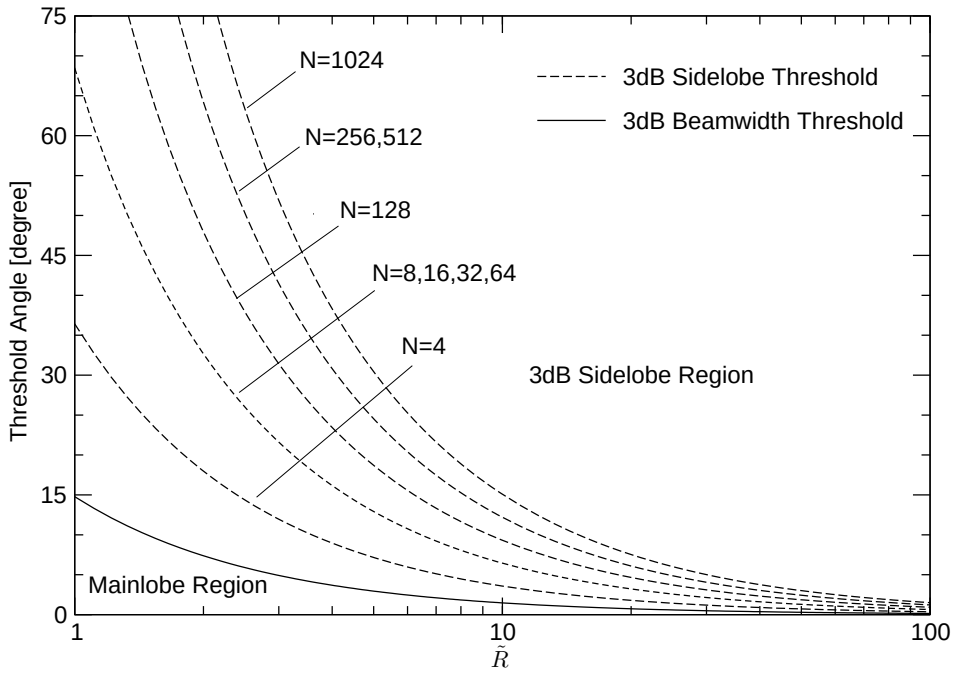

Fig. 5. Threshold of 3 dB beamwidth and 3 dB sidelobe region with respect to $\tilde{R}$ and number of nodes N.

$P(\phi|\boldsymbol{z})$ of (12) into the above, as

$$D(\boldsymbol{z}) = \left[\frac{1}{N} + \frac{1}{N^2} \sum_{k=1}^{N} \sum_{\substack{l=1 \\ l \neq k}}^{N} J_0 \left(4\pi \tilde{R}(z_k - z_l) \right) \right]^{-1}. \tag{28}$$

The mean value of (28) is given by

$$D_{\text{av}} \triangleq E_{\boldsymbol{z}}[D(\boldsymbol{z})]. \tag{29}$$

Unfortunately, direct calculation of (29) does not result in a closed-form or insightful expression. Thus, we shall consider the following as an alternative measure:

$$\tilde{D}_{\text{av}} \triangleq \frac{2\pi}{\int_{-\pi}^{\pi} E_{\boldsymbol{z}}[P(\phi|\boldsymbol{z})] d\phi} = \frac{2\pi}{\int_{-\pi}^{\pi} P_{\text{av}}(\phi) d\phi}. \tag{30}$$

Note that by Jensen's inequality, we have

$$\tilde{D}_{\text{av}} \leq D_{\text{av}}, \tag{31}$$

which means that $\tilde{D}_{\text{av}}$ in (29) is a lower bound on D_{av}. However, since by the law of large numbers the denominator of $D(\boldsymbol{z})$ may approach its average value with high probability as N increases, the above bound is expected to become tight as N increases. This will be verified in the numerical results below.

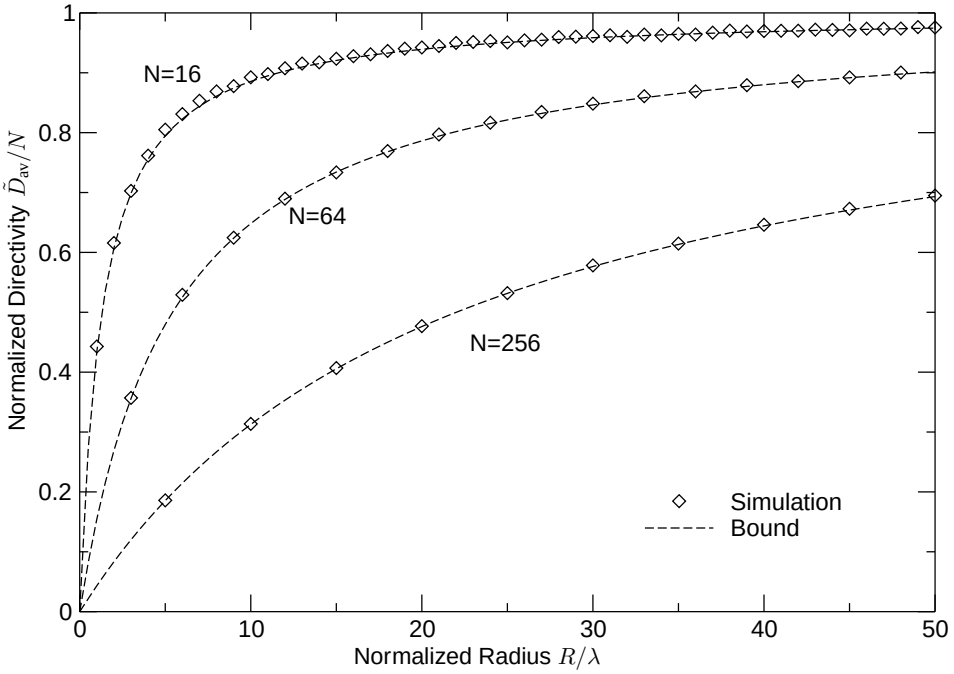

Fig. 6. The relationship between directivity $\tilde{D}_{\text{av}}/N$ and normalized radius $\tilde{R}$.

Substituting (15) into the above, we obtain[2]

$$\tilde{D}_{\text{av}} = \frac{N}{1 + (N-1)\,{}_2F_3\left(\frac{1}{2}, \frac{3}{2}\,;\, 1, 2, 3\,;\, -(4\pi\tilde{R})^2\right)}, \tag{32}$$

where ${}_2F_3\left(\frac{1}{2}, \frac{3}{2}\,;\, 1, 2, 3\,;\, -x^2\right)$ is a generalized hypergeometric function which monotonically decreases with increasing x and converges to 0 as $x \to \infty$. Therefore, unlike well-designed deterministic linear arrays, the gain of a given realization is very likely to be less than N, and the limit N can be approached only by increasing $\tilde{R}$. This agrees with the previous observation that the average mainbeam becomes narrow as $\tilde{R}$ increases and thus improves the directivity.

Fig. 6 shows the relationship between the normalized directivity bound $\tilde{D}_{\text{av}}/N$ and $\tilde{R}$. Also shown in the figure as diamond-shaped points are the corresponding exact average directivities D_{av}/N obtained by the simulation of 1000 realizations. As can be observed, the bound is very tight compared to the exact performance. Thus, it follows that in order to achieve high normalized directivity (i.e. directivity close to N) with N nodes, the distribution of the nodes should be as sparse as possible. In fact, we have the following theorem:

[2]Although (32) is a simple form and offers some insight on asymptotic behavior of directivity, the calculation of the generalized hypergeometric function involved in (32) becomes numerically unstable as $\tilde{R}$ increases, and it is much easier to compute the numerical integration of (30) directly.

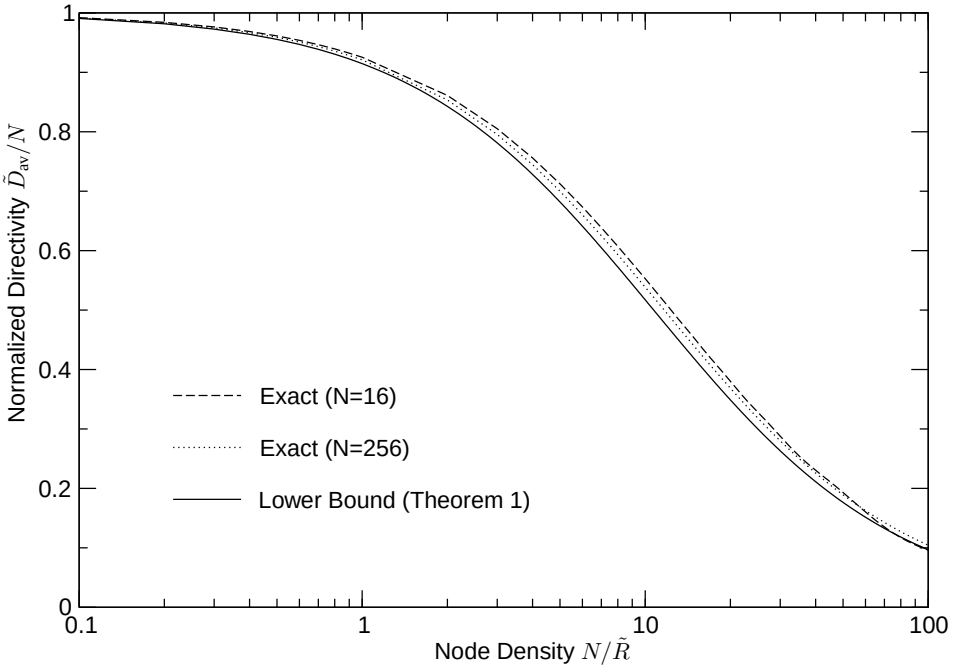

Fig. 7. The relationship between directivity $\tilde{D}_{\text{av}}/N$ and node density $N/\tilde{R}$.

Theorem 1 (Normalized Directivity Lower Bound): For large $\tilde{R}$ and N, D_{av}/N is lower bounded by

$$\frac{D_{\text{av}}}{N} \geq \frac{1}{1+\mu\frac{N}{\tilde{R}}}, \tag{33}$$

where μ is a positive constant independent of N and $\tilde{R}$ ($\mu \approx 0.09332$).

Proof: See Appendix I. ■

Note that the factor $N/\tilde{R}$ can be seen as a *one-dimensional node density*. To verify the above theorem, Fig. 7 shows the relationship between $\tilde{D}_{\text{av}}/N$ and the node density $N/\tilde{R}$, as well as the lower bound in (33).

The above theorem indicates that there is a simple relationship between directivity and node density. It can be seen that the node density almost uniquely determines the normalized directivity D_{av}/N. It is important to note that in order to achieve a certain normalized directivity with a large number of nodes N, the node density should be maintained to the desired value by spreading the nodes as sparsely as possible. Alternatively, if the normalized region $\tilde{R}$ is fixed, it is not efficient in terms of normalized directivity to increase the number of sensor nodes.

The above theorem also indicates that if the sensor nodes are uniformly distributed and if we are to choose N nodes out of them, in terms of normalized directivity it may be better to choose them as sparsely as possible.

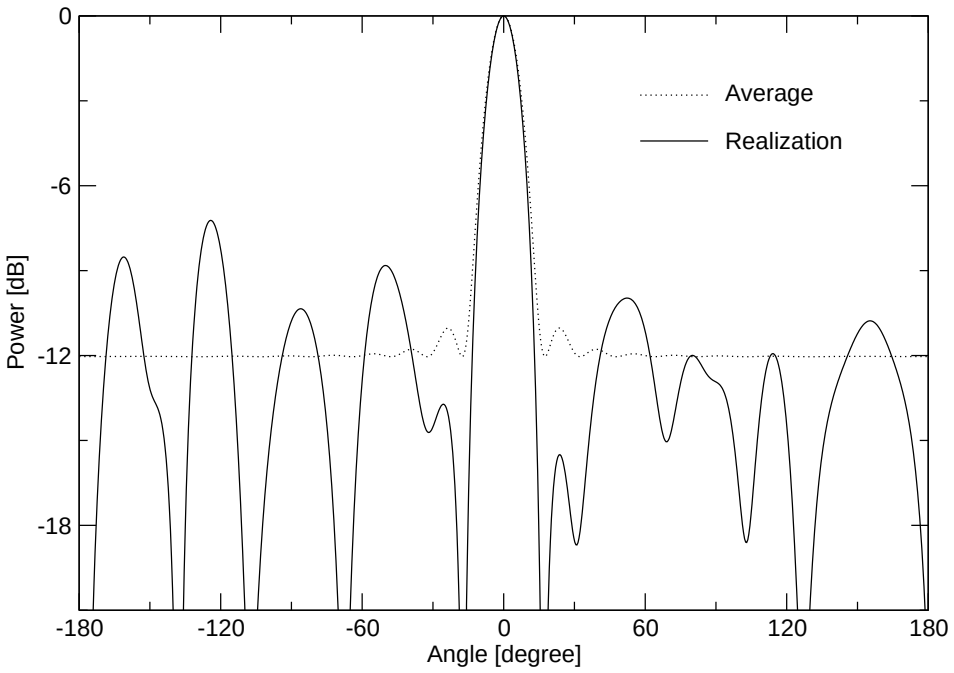

Fig. 8. Average and realization of beampattern with $\tilde{R} = 2$ and $N = 16$.

IV. Distribution of Far-Field Beampattern of Collaborative Beamforming with Perfect Phase Information

In the previous section, we have seen that random arrays have nice average beampatterns with low sidelobes. However, the average behavior does not necessarily represent a beampattern of any given realization unless $N \to \infty$ (and even then, only with probability 1). In fact, even though the average beampattern has a sharp mainbeam and sidelobes always close to $1/N$, there is a large dynamic range of sidelobes among randomly generated beampatterns. As an example, the average beampattern and one particular realization of randomly generated sensor locations is shown in Fig. 8. The mainbeam of the realization closely matches the average, but sidelobes may fluctuate with a large dynamic range and easily exceed the average level.

Therefore, in practice, the statistical *distribution* of beampatterns and sidelobes in particular, is of interest. By approximating the beampattern sidelobes as a complex Gaussian process, Lo [3] has derived the distribution of the beampattern in the case of linear random arrays.

In the following, we first derive a numerical method that allows calculation of the exact distribution of the beampattern without applying Gaussian approximations. We then derive a convenient asymptotic form of the sidelobe distribution using a Gaussian approximation similar to [3], and evaluate its validity in our framework.

A. Exact Evaluation of Distribution

Since the array factor is a sum of i.i.d. random variables, its distribution can be computed numerically by the characteristic function method. To this end, from (11) let

$$\tilde{F}(\phi|\boldsymbol{z}) = \frac{1}{N}\sum_{k=1}^{N}(\tilde{x}_k - j\tilde{y}_k) \triangleq \frac{1}{N}\left(\tilde{X} - j\tilde{Y}\right), \tag{34}$$

where

$$\tilde{x}_k \triangleq \cos\left(z_k\alpha(\phi)\right), \quad \tilde{y}_k \triangleq \sin\left(z_k\alpha(\phi)\right) \tag{35}$$

and $\alpha(\phi)$ is defined in (13). The joint characteristic function of $\tilde{x}_k$ and $\tilde{y}_k$ is given by

$$\Phi_{\tilde{x}_k,\tilde{y}_k}(\omega,\nu) = E_{\tilde{x}_k,\tilde{y}_k}\left[e^{j(\omega\tilde{x}_k - \nu\tilde{y}_k)}\right] = E_{z_k}\left[e^{j[\omega\cos(z_k\alpha(\phi)) - \nu\sin(z_k\alpha(\phi))]}\right]. \tag{36}$$

For a given pair of ω and ν, the above expectation is a single integral of a well-behaved function and can be calculated numerically.

Since $\tilde{F}(\phi|\boldsymbol{z})$ is a sum of N i.i.d. complex random variables, the joint probability density of $\tilde{X}$ and $\tilde{Y}$ in (34) is given by

$$f_{\tilde{X},\tilde{Y}}(x,y) = \left(\frac{1}{2\pi}\right)^2 \int_{-\infty}^{\infty}\int_{-\infty}^{\infty} \Phi^N_{\tilde{x}_k,\tilde{y}_k}(\omega,\nu)e^{-j(\omega x+\nu y)}\,d\omega\,d\nu. \tag{37}$$

The above integral can be computed efficiently using the two-dimensional Fast Fourier Transform (FFT). Finally, the complementary cumulative distribution function (CCDF) of the beampattern, i.e., the probability that the instantaneous power of a given realization in the direction ϕ exceeds the threshold power, P_0, is given by

$$\Pr\left[P(\phi) > P_0\right] = \Pr\left[\frac{\tilde{X}^2 + \tilde{Y}^2}{N^2} > P_0\right] = \iint_{x^2+y^2>N^2P_0} f_{\tilde{X},\tilde{Y}}(x,y)\,dx\,dy. \tag{38}$$

B. Gaussian Approximation of Distribution

The exact evaluation of the CCDF outlined above is computationally demanding, especially if the desired numerical precision is high. Considering that the array factor consists of a sum of N statistically independent random variables, as N increases, by the central limit theorem we may expect that the array factor with any given direction, except at the deterministic angle $\phi = 0$, approaches a complex Gaussian distribution. This approximation may typically result in a simpler distribution formula. To this end, we write (34) as

$$\tilde{F}(\phi|\boldsymbol{z}) = \frac{1}{\sqrt{N}}\left(X - jY\right) \tag{39}$$

where

$$X \triangleq \frac{1}{\sqrt{N}} \sum_{k=1}^{N} \cos\left(z_k \alpha(\phi)\right), \quad Y \triangleq \frac{1}{\sqrt{N}} \sum_{k=1}^{N} \sin\left(z_k \alpha(\phi)\right). \tag{40}$$

Since the z_k's are i.i.d. random variables, as N increases the distribution of X and Y at the direction $\pi \geq |\phi| > 0$ may approach that of a Gaussian with

$$E[X] = 2\frac{J_1\left(\alpha(\phi)\right)}{\alpha(\phi)}\sqrt{N} \triangleq m_x \tag{41}$$

$$\text{VAR}[X] = \frac{1}{2}\left(1 + \frac{J_1\left(2\alpha(\phi)\right)}{\alpha(\phi)}\right) - \left[2\frac{J_1\left(\alpha(\phi)\right)}{\alpha(\phi)}\right]^2 \triangleq \sigma_x^2 \tag{42}$$

$$E[Y] = 0 \tag{43}$$

$$\text{VAR}[Y] = \frac{1}{2}\left(1 - \frac{J_1\left(2\alpha(\phi)\right)}{\alpha(\phi)}\right) \triangleq \sigma_y^2. \tag{44}$$

Note that X and Y are orthogonal and thus statistically uncorrelated. The joint pdf of X and Y is then given by

$$f_{X,Y}(x,y) = \frac{1}{2\pi\sigma_x\sigma_y} \exp\left(-\frac{|x-m_x|^2}{2\sigma_x^2} - \frac{y^2}{2\sigma_y^2}\right). \tag{45}$$

The CCDF of P_0 can be expressed as

$$\begin{aligned}
\Pr\left[P(\phi) > P_0\right] &= \Pr\left[\frac{X^2+Y^2}{N} > P_0\right] = \Pr\left[\sqrt{X^2+Y^2} > \sqrt{NP_0}\right] \\
&= \int_{\sqrt{NP_0}}^{\infty}\int_{-\pi}^{\pi} \frac{r}{2\pi\sigma_x\sigma_y} \exp\left(-\frac{|r\cos\omega - m_x|^2}{2\sigma_x^2} - \frac{r^2\sin^2\omega}{2\sigma_y^2}\right) d\omega\, dr \\
&= \int_{-\pi}^{\pi} \frac{1}{4\pi\sigma_x\sigma_y U_\omega^2} e^{V_\omega^2 - \frac{m_x^2}{2\sigma_x^2}} \left[\sqrt{\pi} V_\omega \ \text{erfc}\left(W_\omega - V_\omega\right) + e^{-(W_\omega - V_\omega)^2}\right] d\omega,
\end{aligned} \tag{46}$$

where

$$U_\omega \triangleq \sqrt{\frac{\cos^2\omega}{2\sigma_x^2} + \frac{\sin^2\omega}{2\sigma_y^2}}, \quad V_\omega \triangleq \frac{m_x\cos\omega}{2\sigma_x^2 U_\omega}, \quad W_\omega \triangleq \sqrt{NP_0}U_\omega. \tag{47}$$

For $\alpha(\phi) \gg 1$, the terms $J_1(2\alpha(\phi))/\alpha(\phi)$ and $|J_1(\alpha(\phi))/\alpha(\phi)|^2$ in the variance expressions (42) and (44) rapidly decrease and their contribution to the resulting variances becomes minor. Therefore, it is very likely that both variances are approximately equal in the sidelobe region. When this is the case, i.e., if $\sigma_x^2 \approx \sigma_y^2 \approx 1/2$, the distribution of the complex envelope becomes a Nakagami-Rice distribution. Consequently, the resulting integral can be expressed by the first-order Marcum-Q function

$$\Pr\left[P(\phi) > P_0\right] = Q\left(\frac{m_x}{\sigma_x}, \frac{\sqrt{NP_0}}{\sigma_x}\right) = Q\left(\sqrt{2}m_x, \sqrt{2NP_0}\right). \tag{48}$$

Furthermore, if the mean $E[X]$ is zero, the envelope follows a Rayleigh distribution and we simply have

$$\Pr\left[P(\phi) > P_0\right] = e^{-NP_0}. \tag{49}$$

C. Mean Value of Array Factor within 3 dB Sidelobe Region

As we have seen, if the mean value of the array factor can be assumed to be zero, the distribution can be significantly simplified and thus analysis becomes readily tractable. From (41) it is apparent that under the constant variance constraint the mean value increases as N increases. Therefore, when N is large, the zero mean assumption may not be guaranteed in general. In Section III-C, we have introduced the 3 dB sidelobe region, and in the following we derive properties of the mean value of the array factor in this region.

From the definition of (24), the sidelobe in the 3 dB region satisfies

$$NP_{\text{av}}(\phi) \leq 2. \tag{50}$$

It follows that

$$\text{VAR}[X] + \text{VAR}[Y] + |E[X]|^2 \leq 2. \tag{51}$$

From (41), (42), and (44), we have

$$1 - \frac{1}{N}|E[X]|^2 + |E[X]|^2 \leq 2, \tag{52}$$

and thus we get

$$|E[X]|^2 \leq \frac{1}{1 - \frac{1}{N}}. \tag{53}$$

Therefore, in the 3 dB sidelobe region, the mean square is bounded by unity in the large-N asymptote and thus the mean does not grow with the number of nodes N.

D. Numerical Comparison

In Fig. 9, the CCDF's computed with various formulae are shown with $\tilde{R} = 2$ and $\phi = \pi/4$, which corresponds to the sidelobe region. The exact formula of (38), the equal variance Gaussian approximation of (48), and the zero-mean Gaussian approximation of (49) are shown in the figure. Note that the exact Gaussian case of (46) was also calculated but is almost identical to (48) for this case and thus is not shown. As observed from Fig. 9, even the zero-mean Gaussian approximation may be valid for this sidelobe region, but for $N = 1024$ the Gaussian approximation will have some noticeable discrepancy with the exact value. This is due to the fact that the zero-mean approximation does not hold for this case. In fact, Fig. 5 indicates that for this value of N, the angle falls between the 3 dB sidelobe region and the mainlobe region and thus the zero mean assumption may not be accurate.

Fig. 10 shows the distribution at 3 dB beamwidth of the average beampattern defined by (23). In this case, (38), (48), and (49) show the different results even for relatively large N, since at this angle the variance of the array factor may be small and thus a large number of random variables is required for its

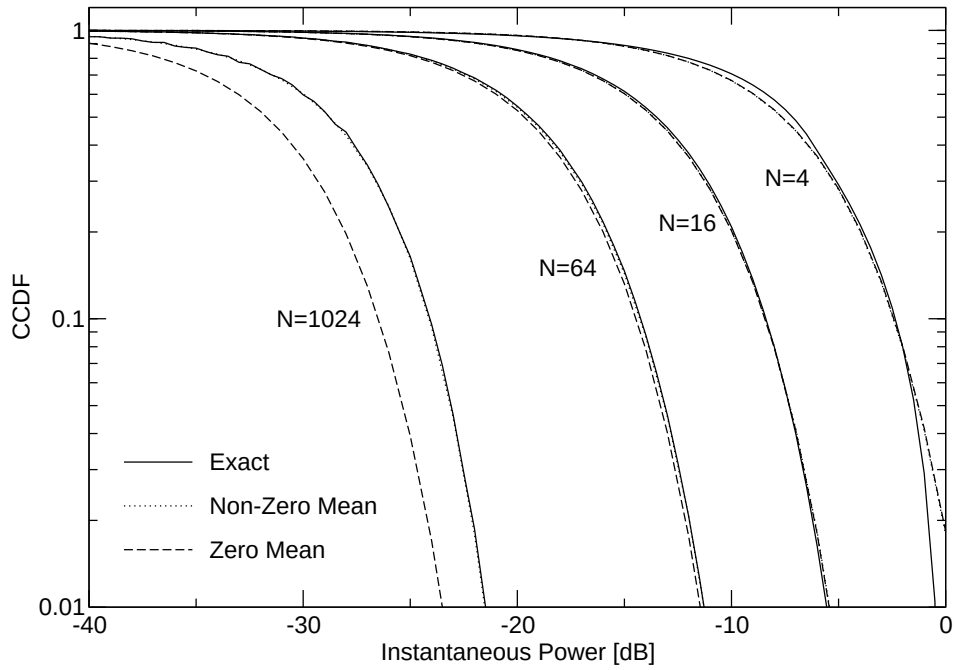

Fig. 9. CCDF of beampattern with $\phi = \pi/4$, and $\tilde{R} = 2$.

convergence toward a non-zero mean Gaussian random variable. As observed, as the number of nodes increases, the mainbeam variance becomes small and approaches the mean value of -3 dB, as expected. Therefore, it can be concluded that for large N, the mainbeam can be made stable. This observation agrees with the result in [3].

V. Distribution of the Maximum of the Sidelobes

It is well known that unlike periodic or equally-spaced antenna arrays, many arrays with unequal spacing will yield no grating lobes for a large number of elements. This property is also preserved for random arrays [3, 8], but in order to verify this, one may need to find the distribution of the maximum power of the sidelobes. In this section, we develop an approximate upper bound on the distribution of the peak sidelobes for random sensor networks.

In the previous section, we have seen that the distribution of the beampattern samples within the sidelobe region can be characterized by a zero mean Gaussian random variable if the zero-mean condition is satisfied. In the following, we further assume that the beam pattern is a Gaussian random *process*. In this case, any two samples taken from the beampattern should be characterized by jointly Gaussian random variables. In the linear random array framework, the distribution of peak sidelobes has been studied in [4–6], assuming the array factor is a Gaussian process. For simplicity, only the 3 dB sidelobe region is considered and it will be assumed that the process is stationary with zero mean. The extension

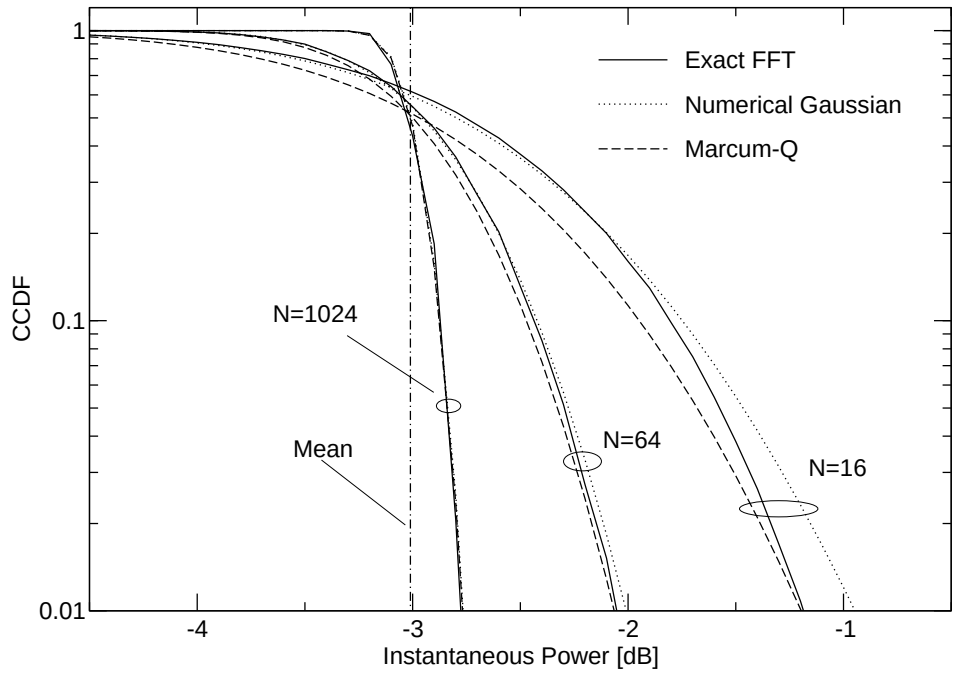

Fig. 10. Distribution of beampattern at $\phi = \phi_{\text{av}}^{\text{3dB}}$ with exact, numerical Gaussian, and Marcum-Q formulas.

to the non-stationary case is studied in [6].

In the following, the CCDF of the maximum peak sidelobe, which is the probability that the maximum peak sidelobe exceeds a given power level, will also be referred to as *outage probability* and denoted by P_{out}.

A. Upper bound on the distribution of peak sidelobe

Let $\nu(a)$ denote the random variable representing the number of upward crossings at a given level a per interval in the 3 dB sidelobe region $\mathcal{S}_{\text{3dB}}$. As shown in Appendix II, assuming that the array factor in this region can be approximated as a zero-mean Gaussian process, the mean of $\nu(a)$ is given by

$$E[\nu(a)] = 4\left(1 - \sin\frac{\phi_{n_0}^{\text{zero}}}{2}\right)\sqrt{\pi}\tilde{R}ae^{-a^2}. \tag{54}$$

Note that the above function monotonically decreases with increasing a only for $a > 1/\sqrt{2}$, and thus is meaningful only in this region. Finally, noticing that the outage probability is the probability that at least one peak exceeds level a and is given by [6]

$$P_{\text{out}} = \Pr\left[\nu(a) \geq 1\right] = \sum_{k=1}^{\infty}\Pr[\nu(a) = k] \leq \sum_{k=1}^{\infty} k\Pr[\nu(a) = k] = E[\nu(a)], \tag{55}$$

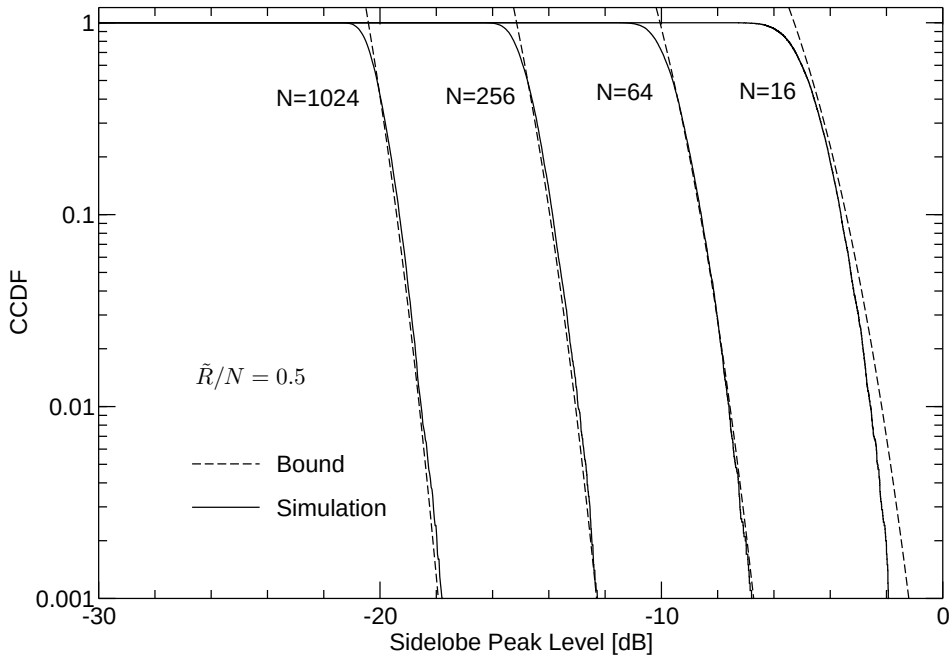

Fig. 11. Comparison of CCDF and upper bound of the sidelobe peaks with $\tilde{R}/N = 0.5$.

(54) serves as an upper bound for the outage probability for the maximum sidelobe peak for $a > 1/\sqrt{2}$. Thus, we obtain the CCDF upper bound as

$$\Pr\left[\max_{\mathcal{S}_{3\text{dB}}} X^2 + Y^2 > P_0\right] \leq 4\left(1 - \sin\frac{\phi_{n_0}^{\text{zero}}}{2}\right)\sqrt{\pi}\tilde{R}\sqrt{NP_0}e^{-NP_0}, \qquad \text{for } NP_0 > \frac{1}{2}. \tag{56}$$

B. Numerical Results

Fig. 11 shows the comparison between simulation results and the upper bound (56). For the simulation, the outage probability is calculated based on 10 000 randomly generated realizations with $\tilde{R}/N = 1/2$ and only the peaks within the 3 dB sidelobe region are examined. Also, in order to capture peak values accurately, the entire 3 dB sidelobe region of ϕ is sampled at a rate as large as $16\pi\tilde{R}$. As can be observed, the bound is in good agreement with simulation for large N.

Let $\tilde{P}_0 = NP_0$ denote the maximum peak value relative to the average sidelobe level. From (56), we have

$$P_{\text{out}} \leq 4\sqrt{\pi}\tilde{R}\sqrt{\tilde{P}_0}e^{-\tilde{P}_0}, \qquad \tilde{P}_0 > 1/2. \tag{57}$$

The above inequality illuminates the relationship between the outage probability and $\tilde{R}$ (assuming that $\phi_{n_0}^{\text{zero}}$ is negligibly small). Fig. 12 shows the maximum possible value of $\tilde{P}_0$ for a given outage probability and $\tilde{R}$. As can be observed, the maximum sidelobe may grow as $\tilde{R}$ increases, but the amount may be below 12 dB for many cases of interest. Consequently, with the normalized sidelobe level $\tilde{P}_0$, the maximum

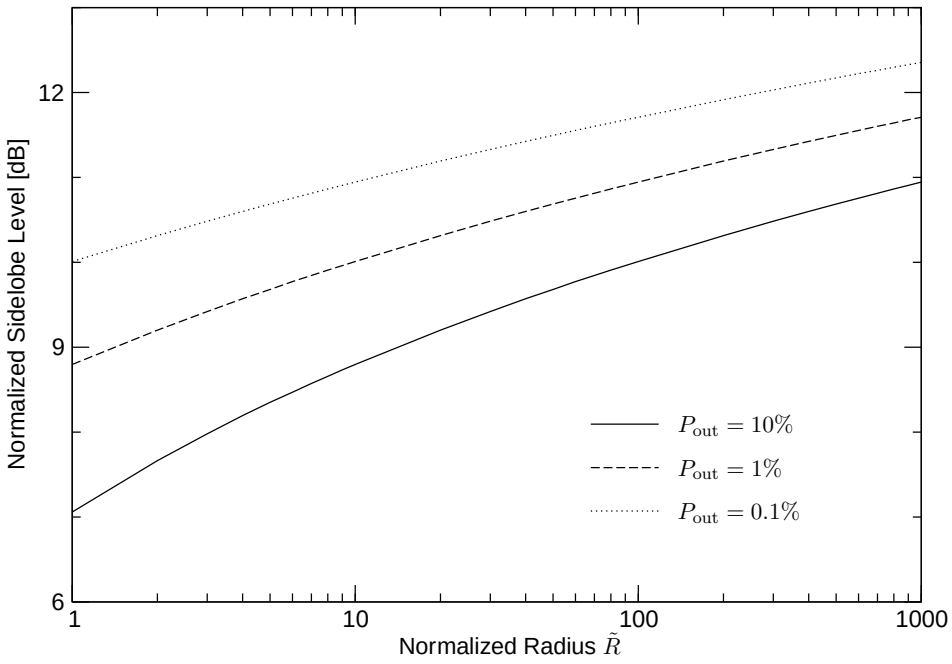

Fig. 12. Bound on sidelobe maximum with a given outage $P_{\rm out}$.

sidelobe level (in the 3 dB region) of the randomly generated arrays may be given by $P_0 = \tilde{P}_0/N$. The required margin $\tilde{P}_0$ depends on the parameters $\tilde{R}$ and $P_{\rm out}$, but not on N. Thus, increasing N always results in a reduction of maximum sidelobe level.

VI. Performance of Distributed Beamforming with Imperfect Phase

So far, we have evaluated the beampattern assuming perfect knowledge of the initial phase for each node. In this section, we analyze the effect of the phase ambiguities in the closed-loop scenario as well as location estimation errors in the open-loop scenario. For each of the two scenarios, we derive the average beampattern and calculate the amount of degradation.

A. Closed-loop case

In the closed-loop case, the effects of imperfect phase may be easily derived, following the approach developed by Steinberg [8]. The initial phase of node k in (2) will now be given by

$$\hat{\Psi}_k = -\frac{2\pi}{\lambda} d_k(\phi_0, \theta_0) + \delta\varphi_k \tag{58}$$

where $\delta\varphi_k$ corresponds to the phase offset due to the phase ambiguity caused by carrier phase jitter or offset between the transmitter and receiver nodes. In the following, the phase offset $\delta\varphi_k$'s are assumed to be i.i.d. random variables. Then, from (3), (4), (5), and (11), the far-field array factor (with $\theta = \theta_0 = \pi/2$)

will be given by

$$\tilde{F}(\phi|\boldsymbol{z},\boldsymbol{\delta\varphi}) = \frac{1}{N}\sum_{k=1}^{N} e^{j\left(-z_k 4\pi\tilde{R}\sin\frac{\phi}{2}+\delta\varphi_k\right)} = \frac{1}{N}\sum_{k=1}^{N} e^{-jz_k 4\pi\tilde{R}\sin\frac{\phi}{2}} e^{j\delta\varphi_k}. \tag{59}$$

The average beampattern of (14) will be replaced by

$$P_{\text{av}}(\phi) \triangleq E_{\boldsymbol{z},\boldsymbol{\delta\varphi}}\left[P(\phi|\boldsymbol{z},\boldsymbol{\delta\varphi})\right]. \tag{60}$$

Similar to (15), direct calculation of (60) results in

$$P_{\text{av}}(\phi) = \frac{1}{N} + \left(1-\frac{1}{N}\right)\left|2\frac{J_1\left(\alpha(\phi)\right)}{\alpha(\phi)}\right|^2 |A_\varphi|^2 \tag{61}$$

where

$$A_\varphi \triangleq E_{\delta\varphi_k}\left[e^{j\delta\varphi_k}\right]. \tag{62}$$

Thus, as $N \to \infty$, the average beampattern will simply become a scaled version of the original by a factor of $|A_\varphi|^2$.

Let us now assume that the phase offset follows a Tikhonov distribution, a typical phase jitter model for phase-locked loop (PLL) circuits, given by [9]

$$f_\varphi(x) = \frac{1}{2\pi I_0\left(1/\sigma_\varphi^2\right)}\exp\left(\cos(x)/\sigma_\varphi^2\right), \qquad |x| \le \pi \tag{63}$$

where σ_φ^2 is the variance of the phase noise and I_n is the nth order modified Bessel function of the first kind. The corresponding attenuation factor is given by

$$A_\varphi = \frac{I_1(1/\sigma_\varphi^2)}{I_0(1/\sigma_\varphi^2)}. \tag{64}$$

The variance of the phase noise σ_φ^2 is related to the loop SNR of the PLL by

$$\rho_\varphi = 1/\sigma_\varphi^2. \tag{65}$$

Fig. 13 shows the degradation factor $|A_\varphi|^2$ with respect to the loop SNR. As observed from the figure, a loop SNR of 5 dB may be necessary for each node in order to reduce the overall beampattern degradation to less than 3 dB.

B. Open-loop case

In the open-loop case, our model of the initial phase is given in (6) with $\theta_0 = \frac{\pi}{2}$, and if there are estimation errors in the location parameters r_k and ψ_k, the initial phase will be replaced by

$$\begin{aligned}\hat{\Psi}_k^\dagger &= \frac{2\pi}{\lambda}(r_k+\delta r_k)\cos(\phi_0-(\psi_k+\delta\psi_k)) \\ &= \frac{2\pi}{\lambda}r_k\cos(\phi_0-(\psi_k+\delta\psi_k)) + \frac{2\pi}{\lambda}\delta r_k\cos(\phi_0-(\psi_k+\delta\psi_k)),\end{aligned} \tag{66}$$

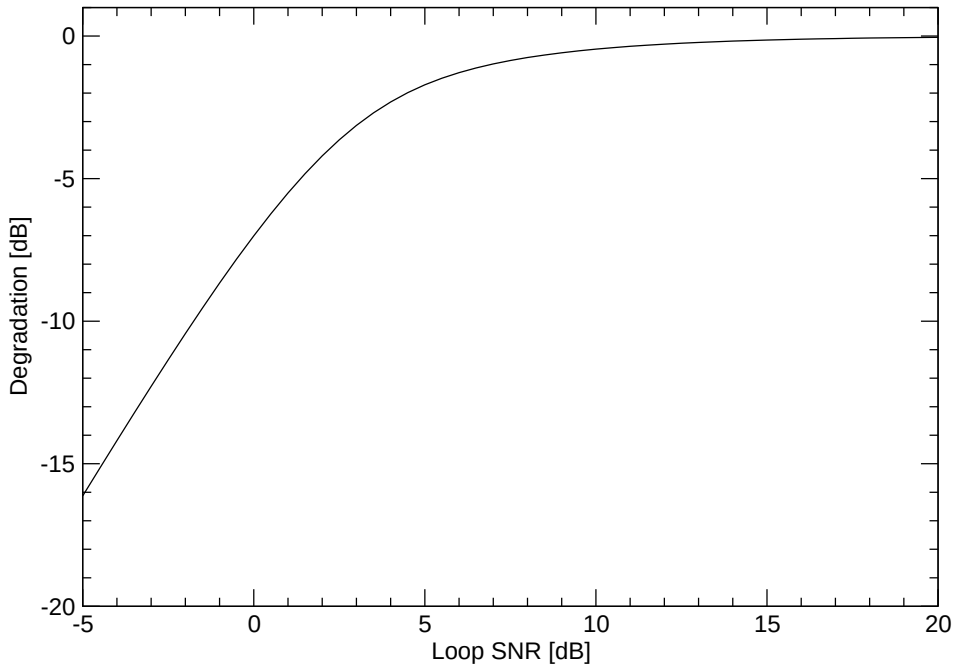

Fig. 13. Mainbeam degradation due to the phase noise in the closed-loop scenario.

where δr_k and $\delta\psi_k$ are the corresponding error random variables, each set assumed to be i.i.d. and also independent of r_k and ψ_k for simplicity. With the far-field approximation, we have

$$\begin{aligned}\frac{2\pi}{\lambda}d_k\left(\phi,\frac{\pi}{2}\right)+\hat{\Psi}_k^{\dagger} &\approx \frac{2\pi}{\lambda}\left\{A-r_k\left[\cos(\phi-\psi_k)-\cos(\phi_0-\psi_k-\delta\psi_k)\right]+\delta r_k\cos(\phi_0-(\psi_k+\delta\psi_k))\right\}\\ &= \frac{2\pi}{\lambda}A+\frac{4\pi}{\lambda}r_k\left[\sin\left(\psi_k-\frac{\phi_0+\phi-\delta\psi_k}{2}\right)\sin\left(\frac{\phi_0-\phi-\delta\psi_k}{2}\right)\right]\\ &\quad+\frac{2\pi}{\lambda}\delta r_k\cos(\psi_k-(\phi_0-\delta\psi_k)).\end{aligned} \tag{67}$$

Let $\tilde{\psi}_k \triangleq \psi_k - \frac{\phi+\phi_0-\delta\psi_k}{2}$. Then, the right-hand side (RHS) of (67) is given by

$$\frac{2\pi}{\lambda}A-\frac{4\pi}{\lambda}r_k\sin\tilde{\psi}_k\sin\left(\frac{\phi-\phi_0-\delta\psi_k}{2}\right)+\frac{2\pi}{\lambda}\delta r_k\cos\left(\tilde{\psi}_k+\frac{\phi-\phi_0+\delta\psi_k}{2}\right). \tag{68}$$

The resultant far-field array factor of (7) will then be given by

$$\tilde{F}^{\dagger}(\phi|\boldsymbol{r},\boldsymbol{\psi},\boldsymbol{\delta\psi},\boldsymbol{\delta r}) = e^{j\frac{2\pi}{\lambda}A}\frac{1}{N}\sum_{k=1}^{N}e^{-j\frac{4\pi}{\lambda}r_k\sin\tilde{\psi}_k\sin\left(\frac{\phi-\phi_0-\delta\psi_k}{2}\right)+j\frac{2\pi}{\lambda}\delta r_k\cos\left(\tilde{\psi}_k+\frac{\phi-\phi_0+\delta\psi_k}{2}\right)}, \tag{69}$$

and the beampattern is expressed as

$$P(\phi|\boldsymbol{z},\boldsymbol{v},\boldsymbol{\delta\psi}) = \frac{1}{N}+\frac{1}{N^2}\sum_{k=1}^{N}\sum_{\substack{l=1\\l\neq k}}^{N}e^{-j4\pi\tilde{R}\left\{z_k\sin\left(\frac{\phi-\phi_0-\delta\psi_k}{2}\right)-z_l\sin\left(\frac{\phi-\phi_0-\delta\psi_l}{2}\right)\right\}}e^{j\frac{2\pi}{\lambda}(v_k-v_l)}, \tag{70}$$

where

$$z_k \triangleq \frac{r_k}{R}\sin\tilde{\psi}_k = \tilde{r}_k \sin\left(\psi_k + \frac{\delta\psi_k}{2} - \frac{\phi+\phi_0}{2}\right) \tag{71}$$

$$v_k \triangleq \delta r_k \cos\left(\tilde{\psi}_k + \frac{\phi+\delta\psi_k}{2}\right) = \delta r_k \cos\left(\psi_k + \delta\psi_k - \phi_0\right). \tag{72}$$

Conditioned on ϕ, ϕ_0 and $\delta\phi_k$, the angle $\tilde{\psi}_k$ can be seen as a uniformly distributed random variable, and thus the pdf of z_k is given by (10). Considering the fact that r_k and δr_k are assumed to be statistically independent, we further assume for analytical purposes that z_k and v_k are statistically independent. Then, again, the beampattern does not depend on the particular choice of ϕ_0. Furthermore, on modeling δr_k as being uniformly distributed over $[-r_{\max}, r_{\max}]$ and assuming the phase term of v_k to be uniformly distributed over $[0, 2\pi]$, the probability density function of v_k will be given by

$$f_{v_k}(v) = \frac{1}{\pi r_{\max}}\left[\ln\left(1+\sqrt{1-\left(\frac{v}{r_{\max}}\right)^2}\right) - \ln\frac{|v|}{r_{\max}}\right], \qquad |v| \le r_{\max} \tag{73}$$

Consequently, the average beampattern can be written as

$$P_{\text{av}}(\phi) = \frac{1}{N} + \left(1-\frac{1}{N}\right)|A_\psi(\phi)|^2\,|A_r|^2, \tag{74}$$

where

$$\begin{aligned} A_r &\triangleq E_{v_k}\left[e^{j\frac{2\pi}{\lambda}v_k}\right] = \frac{2}{\pi}\int_0^1 \cos\left(\frac{2\pi}{\lambda}r_{\max}t\right)\ln\frac{1+\sqrt{1-t^2}}{t}dt \\ &= {}_1F_2\left(\frac{1}{2}\,;\,1,\frac{3}{2}\,;\,-\left(\pi\frac{r_{\max}}{\lambda}\right)^2\right) \end{aligned} \tag{75}$$

$$A_\psi(\phi) \triangleq E_{z_k,\delta\psi_k}\left[e^{j4\pi\tilde{R}z_k\sin\left(\frac{\phi_0+\delta\psi_k-\phi}{2}\right)}\right] = E_{\delta\psi_k}\left[\frac{J_1\left(4\pi\tilde{R}\sin\frac{\phi-\delta\psi_k}{2}\right)}{2\pi\tilde{R}\sin\frac{\phi-\delta\psi_k}{2}}\right], \tag{76}$$

and without loss of generality $\phi_0 = 0$ was assumed. In (75), ${}_1F_2\left(\frac{1}{2}\,;\,1,\frac{3}{2}\,;\,-x^2\right)$ denotes a generalized hypergeometric function which has an oscillatory tail but converges to zero as x increases.

Also, assuming that the $\delta\psi_k$ are uniformly distributed over $[-\psi_{\max}, \psi_{\max}]$ and using the approximation $\sin(\phi+\delta\psi_k) \approx \phi + \delta\psi_k$ which is valid for the beampattern around the mainbeam, we obtain

$$\begin{aligned} A_\psi(\phi) \approx{}& \frac{1}{2}\left(1-\frac{\phi}{\psi_{\max}}\right){}_1F_2\left(\frac{1}{2}\,;\,\frac{3}{2},2\,;\,-(\pi\tilde{R}(\phi+\psi_{\max}))^2\right) \\ &+ \frac{1}{2}\left(1+\frac{\phi}{\psi_{\max}}\right){}_1F_2\left(\frac{1}{2}\,;\,\frac{3}{2},2\,;\,-(\pi\tilde{R}(\phi-\psi_{\max}))^2\right). \end{aligned} \tag{77}$$

Since the hypergeometric function ${}_1F_2\left(\frac{1}{2}\,;\,\frac{3}{2},2\,;\,-x^2\right)$ has a maximum peak value of 1 at $x=0$, the above expression indicates that regardless of the value of $\tilde{R}$, there may be two symmetric peaks around

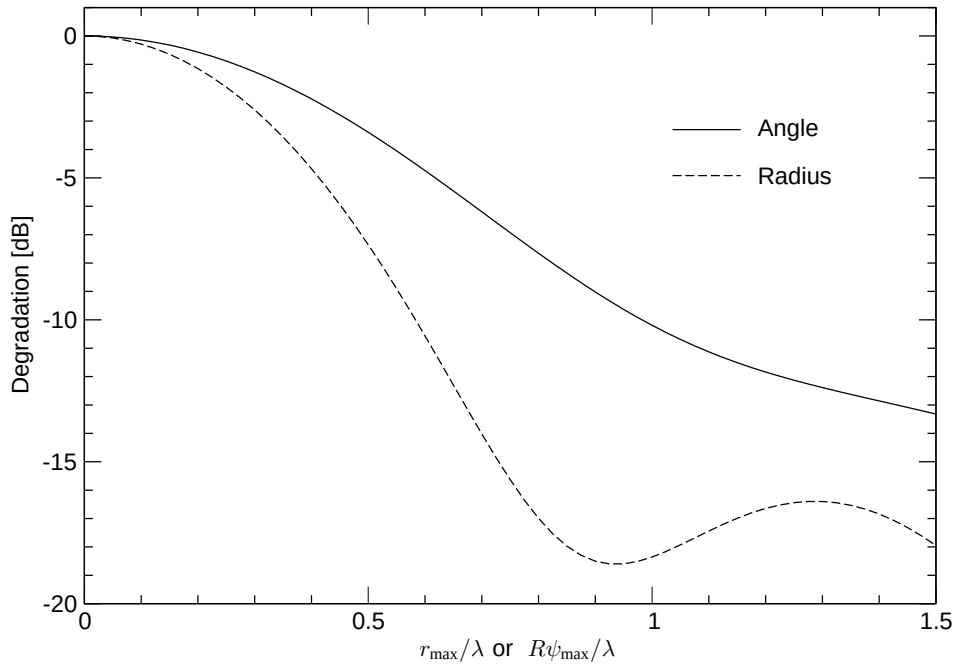

Fig. 14. Mainbeam degradation due to location estimation errors in open-loop scenario.

the mainbeam at $\phi = \pm\psi_{\max}$ resulting in a *pointing error*. Therefore, the mainbeam may spread over by a factor of $\psi_{\max}$. At the center of the mainbeam, we have

$$A_\psi(0) = {}_1F_2\left(\frac{1}{2}\,;\,\frac{3}{2}, 2\,;\,-\left(\pi\frac{R\psi_{\max}}{\lambda}\right)^2\right). \tag{78}$$

Fig. 14 shows the degradation factor $|A_r|^2$ and $|A_\psi(0)|^2$ for a given $\frac{r_{\max}}{\lambda}$ and $\frac{R\psi_{\max}}{\lambda}$. As observed from the figure and discussion above, the angle estimation error has two effects, i.e., pointing error and mainbeam degradation. In particular, if we wish to suppress the degradation below 3 dB, from the figure, we should choose $R\psi_{\max}/\lambda \leq 1/2$. This means that the maximum angle estimation error should satisfy

$$\psi_{\max} \leq \frac{\lambda}{2R} = \frac{1}{2\tilde{R}}, \tag{79}$$

and as $\tilde{R}$ becomes large, the requirement of minimum angle ambiguity from (79) becomes severe.

VII. Conclusion

In this paper, we have analyzed the stochastic performance of random arrays for distributed collaborative beamforming, in the framework of wireless ad hoc sensor networks. It has been shown that under ideal channel and system assumptions, directivity of order N can be achieved asymptotically with N sensor nodes, as long as the sensor nodes are located sparsely enough. We studied the average and the distribution of the beampattern as well as the distribution of the sidelobe peaks. Several forms of the CCDF of the

beampattern have been derived and compared, with particular emphasis on the Gaussian approximation of the array factor. We have considered two scenarios of distributed beamforming and investigated the effects of phase ambiguity and location estimation error upon the resultant average beampatterns.

Our main conclusion is that, given a number of nodes randomly distributed over a large disk, one may form a nice beampattern with narrow mainlobe and sidelobes as low as $1/N$ plus some margin for maximum sidelobe peaks. Also, the directivity approaches N if the nodes are located as sparsely as possible. However, our analysis is based on a number of ideal assumptions on the system and channel model. In practice, a number of open issues remain, such as applicability of beamforming when the destination or nodes in the cluster are in rapid motion or the channel suffers severe multipath fading. Also, specific algorithms should be developed for frequency offset correction of each node as well as methods for initial phase or location estimation. Finally, efficient protocols for sharing the transmit as well as calibration information among nodes are required.

APPENDIX I
PROOF OF THEOREM 1

We first prove the following lemma:

Lemma 1: A generalized hypergeometric function ${}_2F_3\left(\frac{1}{2},\frac{3}{2};\,1,2,3;\,-x^2\right)$ with $x \gg 1$ can be bounded as

$$f(x) \triangleq {}_2F_3\left(\frac{1}{2},\frac{3}{2};\,1,2,3;\,-x^2\right) \le \frac{c_0}{x} \tag{80}$$

where c_0 is a constant ($c_0 \approx 1.1727$).

Proof: We start with the integral form

$$f(x) = \frac{1}{\pi}\int_0^{\pi}\left|2\frac{J_1\left(x\sin\frac{\theta}{2}\right)}{x\sin\frac{\theta}{2}}\right|^2 d\theta = \frac{1}{\pi}\int_0^{x}\left|2\frac{J_1(t)}{t}\right|^2 \frac{2}{\sqrt{x^2-t^2}}dt. \tag{81}$$

Since the asymptotic form of $J_1(x)$ given by (16) is valid for $x \gg 1$, we have the following inequalities

$$\left|2\frac{J_1(t)}{t}\right|^2 \le \cos^2(\alpha_0 t), \qquad \text{for } t \le x_0 \tag{82}$$

$$\int_t^{t+\Delta}\left|2\frac{J_1(u)}{u}\right|^2 du \le \int_t^{t+\Delta}\frac{8}{\pi u^3}\,du, \qquad \text{for } t > x_0 \tag{83}$$

for some threshold value x_0 which should be determined numerically, and for an appropriate interval $\Delta > 0$. The parameter α_0 can be chosen such that

$$\cos(\alpha_0 x_0) = \sqrt{\frac{8}{\pi x_0^3}}, \tag{84}$$

should hold, and this guarantees a continuity of the function at the threshold $t = x_0$. Fig. 15 illustrates the relationship of (82) and (83) with x_0 chosen as a cross point of t between the functions $J_1(t)$ and

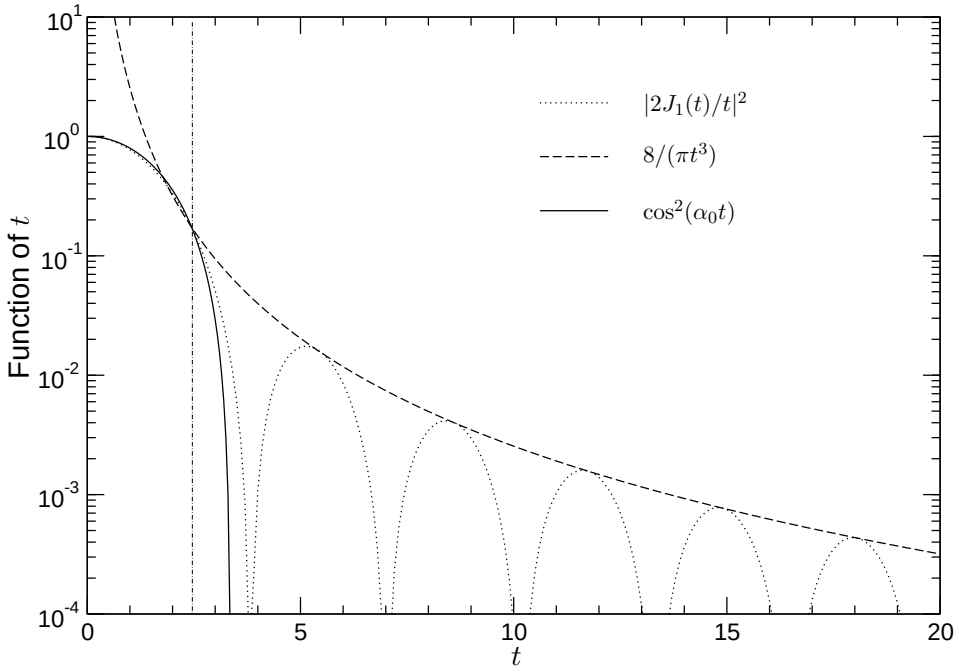

Fig. 15. Function $|2J_1(t)/t|^2$ and its upper bound with $x_0 = 2.4445$.

$\sqrt{2/(\pi t)}$, yielding $x_0 = 2.4445$. The corresponding value of α_0 is 0.4664. Substituting (82) and (83) into (81), we get for $x > x_0$

$$f(x) \le \frac{2}{\pi}\int_0^{x_0} \frac{\cos^2(\alpha_0 t)}{\sqrt{x^2-t^2}}dt + \frac{16}{\pi^2}\int_{x_0}^{x} \frac{1}{t^3\sqrt{x^2-t^2}}dt. \tag{85}$$

The first term on the RHS of (85) is given by

$$\begin{aligned}\frac{2}{\pi}\int_0^{x_0} \frac{\cos^2(\alpha_0 t)}{x\sqrt{1-\left(\frac{t}{x}\right)^2}}dt &= \frac{2}{\pi x}\int_0^{x_0}\left\{1+\frac{1}{2}\left(\frac{t}{x}\right)^2 + O\left(1/x^4\right)\right\}\cos^2(\alpha_0 t)dt \\ &= \frac{1}{\pi x}\left(x_0 + \frac{\sin(2\alpha_0 x_0)}{2\alpha_0}\right) + O\left(1/x^3\right).\end{aligned} \tag{86}$$

The second term on the RHS of (85) is given by

$$\begin{aligned}\frac{16}{\pi^2}\int_{x_0}^{x} \frac{1}{t^3\sqrt{x^2-t^2}}dt &= \frac{16}{\pi^2}\left[\frac{1}{x}\frac{\sqrt{1-\left(\frac{x_0}{x}\right)^2}}{2x_0^2} + \frac{1}{2x^3}\left\{\ln\left(1+\sqrt{1-\left(\frac{x_0}{x}\right)^2}\right) + \ln\left(\frac{x}{x_0}\right)\right\}\right] \\ &= \frac{8}{\pi^2 x_0^2}\frac{1}{x}\left(1-\left(\frac{x_0}{x}\right)^2 + O\left(1/x^4\right)\right) + O\left(\ln(x)/x^3\right) \\ &= \frac{1}{x}\frac{8}{\pi^2 x_0^2} + O\left(\ln(x)/x^3\right).\end{aligned} \tag{87}$$

Consequently, we may write

$$f(x) \le \frac{1}{\pi}\left(x_0 + \frac{\sin(2\alpha_0 x_0)}{2\alpha_0} + \frac{8}{\pi x_0^2}\right)\frac{1}{x} + O\left(\ln(x)/x^3\right) \tag{88}$$

and the second term on the RHS of (88) drops as x becomes large. With $x_0 = 2.4445$ and $\alpha_0 = 0.4664$, the coefficient of $1/x$ can be calculated to be $c_0 = 1.1727$. ■

Proof: [Proof of Theorem 1] From (31), (32), and Lemma 1, we have

$$\frac{D_{\text{av}}}{N} \geq \frac{\tilde{D}_{\text{av}}}{N} \geq \frac{1}{1+(N-1)\frac{c_0}{4\pi\tilde{R}}} = \frac{1}{1+\left(1-\frac{1}{N}\right)\frac{c_0}{4\pi}\frac{N}{\tilde{R}}}. \tag{89}$$

For large N, the RHS of (89) converges to (33) with $\mu = \frac{c_0}{4\pi} \approx 0.09332$. ■

APPENDIX II
THE MEAN NUMBER OF UPWARD LEVEL CROSSINGS OF A GAUSSIAN PROCESS

In this appendix, we obtain the mean number of upward crossings of a given level of the zero mean Gaussian process based on the approach of Rice [10, 11]. Assume that X and Y are uncorrelated zero-mean Gaussian processes with variance $\sigma_x^2 = \sigma_y^2 = 1/2$. Let $u = \sin\left(\frac{\phi}{2}\right)$ and X' and Y' denote the corresponding processes differentiated by u. By assumption, X' and Y' become zero mean Gaussian processes. In order to calculate the variance, first consider the autocorrelation function of X at instants $u = u_1$ and u_2 given by

$$\begin{aligned}\rho_X(u_1,u_2) &= E_z\left[\cos\left(z4\pi\tilde{R}u_1\right)\cos\left(z4\pi\tilde{R}u_2\right)\right] + \text{other terms} \\ &= \frac{1}{2}E_z\left[\cos\left(z4\pi\tilde{R}\,(u_1+u_2)\right)\right] + \frac{1}{2}E_z\left[\cos\left(z4\pi\tilde{R}\,(u_1-u_2)\right)\right]\end{aligned} \tag{90}$$

where the other terms become zero by the zero mean assumption. Also for the same reason, the first term of the RHS of (90) may be also approximated by zero. Therefore, letting $v = u1 - u2$, we obtain

$$\rho_X(v) \approx \frac{1}{2}E_z\left[\cos\left(z4\pi\tilde{R}\,(v)\right)\right]. \tag{91}$$

Differentiating the above with respect to v twice, setting $v = 0$ and carrying out the statistical average with respect to z, the variance of X' is given by [12]

$$\sigma_{x'}^2 = -\rho_X''(0) = 2\pi^2\tilde{R}^2. \tag{92}$$

Likewise, one may obtain $\sigma_{y'}^2 = \sigma_{x'}^2$, and the joint pdf of X, X', Y, Y' is given by

$$f_{X,Y,X',Y'}(x,y,x',y') = \frac{1}{(2\pi)^2\sigma_x^2\sigma_{x'}^2}\exp\left(-\frac{x^2+y^2}{2\sigma_x^2} - \frac{x'^2+y'^2}{2\sigma_{x'}^2}\right) \tag{93}$$

On changing the random variables in the polar coordinates via $X = \Omega\cos\Theta$, $Y = \Omega\sin\Theta$ and integrating out Θ and Θ', we obtain

$$f_{\Omega,\Omega'}(\omega,\omega') = \omega e^{-\omega^2}\frac{1}{\sqrt{\pi}\pi\tilde{R}}e^{-\frac{\omega'^2}{4\pi^2\tilde{R}^2}}. \tag{94}$$

The number of positive (upward) crossings of the process ω at level a per interval du is given by [10, 11]

$$\nu(a)du = du\int_0^\infty \omega' f_{\Omega,\Omega'}(a,\omega')d\omega' = du\,2\sqrt{\pi}\tilde{R}ae^{-a^2} \tag{95}$$

Consequently, the mean number of upward crossings for the interval $\mathcal{S}_{\text{3dB}}$ is given by

$$E[\nu(a)] = \int_{u=\sin\left(\frac{\phi}{2}\right),\phi\in\mathcal{S}_{\text{3dB}}} du\ \nu(a), \tag{96}$$

which results in (54).

REFERENCES

[1] K. Yao, R. E. Hudson, C. W. Reed, D. Chen, and F. Lorenzelli, "Blind beamforming on a randomly distributed sensor array system," *IEEE J. Select. Areas Commun.*, vol. 16, pp. 1555–1567, Oct. 1998.

[2] J. C. Chen, L. Yip, J. Elson, H. Wang, D. Maniezzo, R. E. Hudson, K. Yao, and D. Estrin, "Coherent acoustic array processing and localization on wireless sensor networks," *Proc. IEEE*, vol. 91, pp. 1154–11162, Aug. 2003.

[3] Y. T. Lo, "A mathematical theory of antenna arrays with randomly spaced elements," *IRE Trans. Antennas Propagat.*, vol. 12, pp. 257–268, May 1964.

[4] B. D. Steinberg, "The peak sidelobe of the phased array having randomly located elements," *IEEE Trans. Antennas Propagat.*, vol. 20, pp. 129–136, Mar. 1972.

[5] V. D. Agrawal and Y. T. Lo, "Mutual coupling in the phased arrays of randomly spaced antennas," *IEEE Trans. Antennas Propagat.*, vol. 20, pp. 288–295, May 1972.

[6] M. B. Donvito and S. A. Kassam, "Characterization of the random array peak sidelobe," *IEEE Trans. Antennas Propagat.*, vol. 27, pp. 379–385, May 1979.

[7] C. A. Balanis, *Antenna Theory: Analysis and Design*. New York: Wiley, 1997.

[8] B. D. Steinberg, *Principles of Aperture & Array System Design*. New York: Wiley, 1976.

[9] A. J. Viterbi, *Principles of Coherent Communication*. New York: McGraw-Hill, 1966.

[10] S. O. Rice, "Mathematical analysis of random noise – Part I," *Bell Syst. Tech. J.*, vol. 23, pp. 282–332, July 1944.

[11] S. O. Rice, "Mathematical analysis of random noise – Part II," *Bell Syst. Tech. J.*, vol. 24, pp. 46–156, Jan. 1945.

[12] H. Cramer and M. R. Leadbetter, *Stationary and Related Stochastic Processes*. New York: Wiley, 1967.